

Observation of two deep, distant (1.4, 4)km impulsive RF transmitters by the Askaryan Radio Array (ARA).

John Kelley*, **Ming Yuan Lu**

University of Wisconsin

David Seckel†, **Yue Pan**

University of Delaware

E-mail: seckel@bartol.udel.edu

David Z. Besson

University of Kansas

for the ARA Collaboration

Full author list: http://ara.wipac.wisc.edu/collaboration/authors/ara_icrc17

The Askaryan Radio Array (ARA) operates two stations (ARA-2, ARA-3) each with 16 antennas deployed on the corners of a cuboid at depths of 175-200 m at South Pole. The antennas are sensitive to either vertical (8 antennas) or horizontal (8 antennas) polarized radiation arriving from in-ice neutrino-induced cascades. At the time of IceCube construction, two calibration pulsers were deployed at a depth of 1400 m on two strings proximal to the ARA stations. These pulsers were operated during the 2014-15 and 2016-17 seasons and were detected as triggered events by ARA stations. The received signals can be used to study the complex ice permittivity at radio frequencies, including attenuation, index of refraction and birefringence. Standard ARA reconstruction of the deep pulser locations validates station geometry, and the index of refraction model used by ARA. We observe clear birefringent effects for horizontally propagating signals in polar ice. We also discuss plans to utilize the open SPiceCore hole to broadcast to existing and planned ARA stations, further characterize the South Pole ice as a function of depth, and test the paradigm of geometric optics for the propagation of electromagnetic meter wavelength radiation through polar ice.

35th International Cosmic Ray Conference

10-20 July, 2017

Bexco, Busan, Korea

*Speaker.

†Corresponding author

1. Introduction

The Askaryan Radio Array[1] (ARA) searches for UHE neutrinos[1, 2, 3, 4] by detecting the radio frequency (RF) radiation from particle cascades produced as a result of neutrino interactions in polar ice. This radiation must propagate from the neutrino interaction vertex to the detector. In the case of ARA, the detector plan consists of 37 independent stations (Figure 1) in a hexagonal array with spacing of 2 km. Of these, three (ARA-1,2,3) were deployed in 2011/12 and 2012/13, and three more (ARA-4,5,6), including one with an advanced trigger system[5], are scheduled for deployment this year 2017/18. The stations are deployed at depths of 175-200 m. Each station includes 16 antennas, 8 sensitive to vertically polarized (Vpol) and 8 sensitive to horizontally polarized (Hpol) radiation, with a bandwidth of approximately 200-700 MHz. The antennas are installed on four strings and define the corners of a cuboid of 20 m height, and 20 m on the horizontal diagonal. At each corner there is a pair of an Hpol antenna sitting 3m above a Vpol antenna. Signals are amplified at the antenna, passed by cable to an in-ice RF over optical fiber link to the surface, and converted back to RF voltage signals before entering the data acquisition system[1].

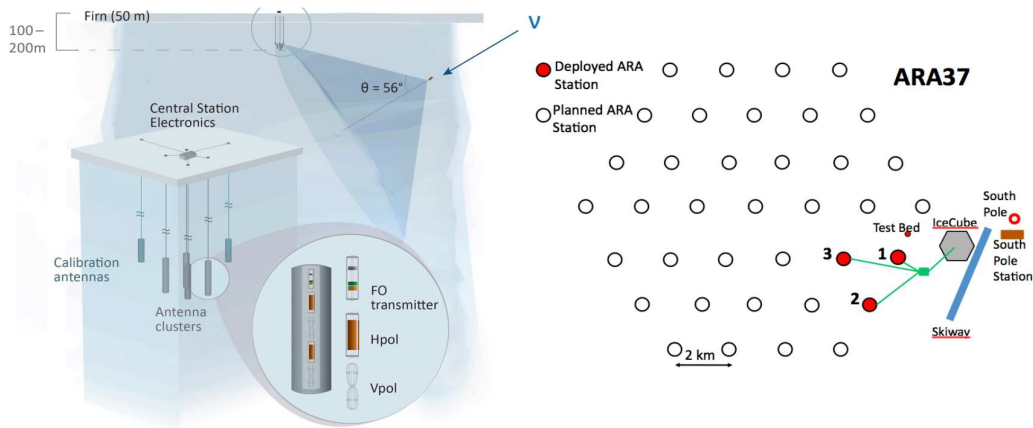


Figure 1: Left: ARA station design (see text). Right: ARA plan. Three stations ARA-4,5,6 are scheduled for deployment in 2017/18. Data from ARA-2,3 are discussed in this proceeding.

An ARA station is sensitive to cascades with $E > 10^{17}$ eV at distances of several hundred meters. The sensitive ice volume increases with energy as intrinsic power overcomes the $1/r^2$ geometry factor and losses due to RF attenuation in ice. In the middle of the cosmogenic neutrino band ($\sim 10^{18.5}$ eV) ARA detects events from several km distance. It is therefore critical to understand the properties of the ice within the array, especially at depths of 1000-2000 m. Anticipating this, during the last year of IceCube construction three pulsers were deployed on IceCube strings 1 (1400 m, 2450 m) & 22 (1400 m), proximal to the planned ARA. The pulser at 2450 m depth was operated in conjunction with the ARA Test Bed[6] to validate the South Pole index of refraction $n(z)$ and RF attenuation[7]. The pulsers (ICS1, ICS22) at depths of 1400 m were operated in 2014/15 as part of the calibration of ARA-2 and ARA-3[8], and again in 2016/17 after the ARA trigger timing was adjusted - enabling capture of an extended waveform and the present analysis.

Figure 2 shows the ARA and IceCube layout, with two rays propagating from ICS1 to ARA-2. The presence of two rays from source to receiver is generic for our geometry. For most geometries

a quasi-direct (QD) ray is upcoming at the station and a quasi-reflected ray (QR) is downgoing. When the source vertex is distant, such as for ICS1 and ARA-2, the QR ray refracts in the firm as the index of refraction $n(z)$ decreases from an asymptotic value of 1.78 to about 1.35 at the surface. The maximum height of the QR ray can be determined from Snell's law and either the launch angle of the ray from the source, or the received angle at the station. The rays shown are for $n(z) = 1.78 - 0.43e^{0.0132z}$ as used by ARA for simulation and analysis.

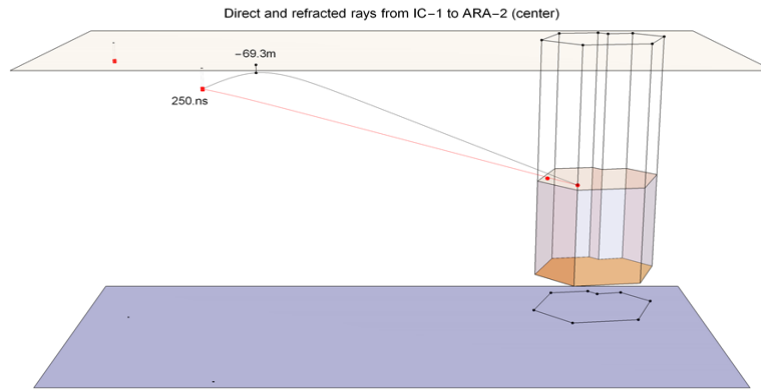


Figure 2: View of ARA-2, ARA-3 and IceCube. The two deep pulsers (ICS1, ICS22) are located at a depth of 1400 m, at a horizontal distance of 3600 m from ARA-2. When a pulser fires the radiation travels to a station via two paths. The “quasi direct” (QD) path is nearly straight. The “quasi-reflected/refracted” (QR) path either reflects off the surface or is refracted in the firm. Both ICS1 and ICS22 can be seen by ARA-2 and ARA-3, although only the rays from ICS1 to ARA-2 are shown. The minimum depth of the QR ray and the difference in arrival times are shown on the figure.

ARA data collection is triggered at a station whenever (3/8 Hpol) OR (3/8 Vpol) antennas go above threshold within a time window (170 ns) inclusive to RF travel time across the station. The thresholds are dynamically adjusted to maintain a constant singles rate, and approximately a combined trigger rate of 5-7 Hz. For any trigger, signals from all 16 antennas are digitized and stored. The readout window for digitization is wide enough to include ~ 100 ns of pre-trigger and ~ 300 ns of post trigger waveform.

Figure 3 shows a deep pulser event. The pulses are emitted from a Vpol antenna and the Vpol response is dominant; however, there is a 10% Hpol signal also received. Moreover, the Hpol signals arrive before the Vpol signals. We discuss this evidence for birefringence in Section 3. Considering just Vpol signals from the same layer, it is evident that string 2 (S2) is closest to the source, followed closely by S4. S3 is furthest from the detector, and as a result its waveform terminates before the arrival of the QR ray. Most antennas show two pulses. The separation between the two pulses is commensurate with the predicted difference in arrival times for pulses traveling along the QD and QR rays from ICS1 to ARA-2. Analysis of the timing (Section 2) validates the station and array geometry, the index of refraction model, and the paradigm of geometric optics operating on multi-km scales. The quality of the pulses is visible from the leading edge. The QD rays travel just through deep ice. Apparently there is little scattering and the leading edge is quite sharp; however, the pulses identified as QR rays have a precursor which may be due to scattering in the firm layer near the top of the pulse trajectory (Figure 2).

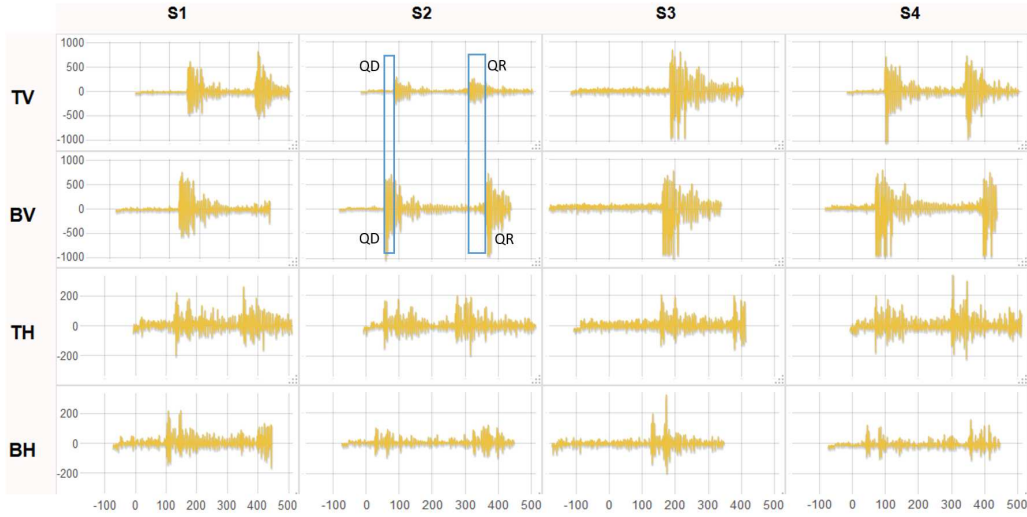


Figure 3: Event display from an ICS1 pulse observed by ARA-2. Each column shows the traces from one string of antennas. Each row shows the traces from one layer of the station. The layers are shown grouped by polarization, but the actual ordering of layers is from the top down, Top Hpol, Top Vpol, Bottom Hpol, Bottom Vpol. The deep pulser broadcasts through a Vpol antenna. The received signals are mainly Vpol, but a 10% signal is seen in Hpol. The arrival times are adjusted for cable delays. The quasi-direct (QD) and quasi-reflected (QR) pulses are identified for S2TV and S2BV, along with timing marks for pulse arrival.

2. Paradigm of geometric optics

Begin by considering the two Vpol antennas on string 2 for which there is only a vertical separation. Label these S2TV and S2BV for top and bottom Vpol. Each channel shows two pulses, one QD and one QR. The QD pulse on S2BV arrives before that on S2TV indicating that the pulse is moving upward as it passes the station. Similarly, the arrival order for QR is reversed indicating a downward ray. These features support the interpretation shown in Figure 2. Using the calibrated station geometry, one can infer the zenith angle of the arriving rays. Similarly, arrival times of other pairs of pulses determine the azimuthal arrival direction. To determine the relative arrival times, we consider the Hilbert envelope of the cross-correlation of the waveforms on two channels. The envelope function reduces sidebands in the correlation function induced by the system bandpass. Figure 4 shows this procedure for S2TV and S2BV. In the present case there are four peaks corresponding to the four possible overlaps of the QD and QR pulses for the two channels. We begin by considering the QD,QD overlap, since that corresponds to normal ARA reconstruction. The analysis presented in [4] proceeds by considering possible source positions on the sky. Through a fast lookup table of arrival times[9], a set of predicted δt_{ij} are produced. These are used to sample the envelopes and give a weight to the proposed δt_{ij} . The most likely position is determined by maximizing the sum of the envelope functions across all pairs of antennas in the event. The result of this procedure is shown in Figure 5 for an ICS22 pulse observed by ARA-3.

The reconstruction from QD rays permits a good direction to the vertex, but determining the distance to the vertex is problematic. This requires a determination of the curvature of the radiation front, which is limited by the modest 20 m baseline of the station. In the present case, however, two rays are detected from the source. Considering the quasi-reflected ray as if it were detected by

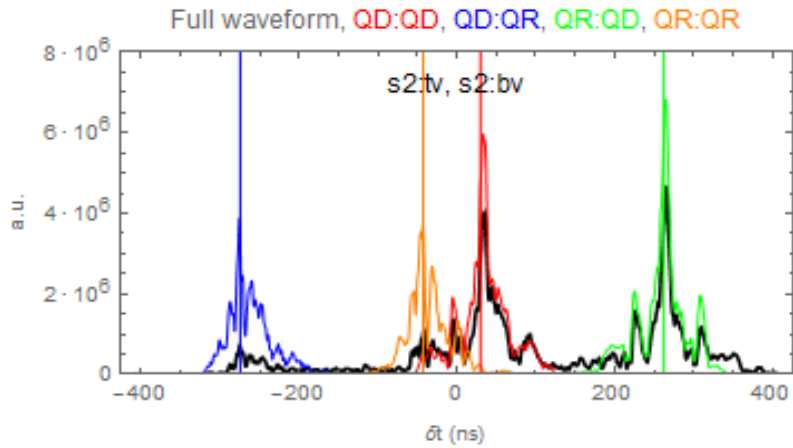


Figure 4: Cross-correlation examples for Vpol antennas S2TV, S2BV. The black curve shows the Hilbert envelope of the cross-correlation function for the full waveform. The colored curves show the same quantity for pulse snips extracted from the full waveform. Vertical lines show the predicted arrival times using the calibrated station geometry, the index of refraction model used both for analysis and simulation, and an array geometry adjusted to account for horizontal changes in the elevation of the snow surface.

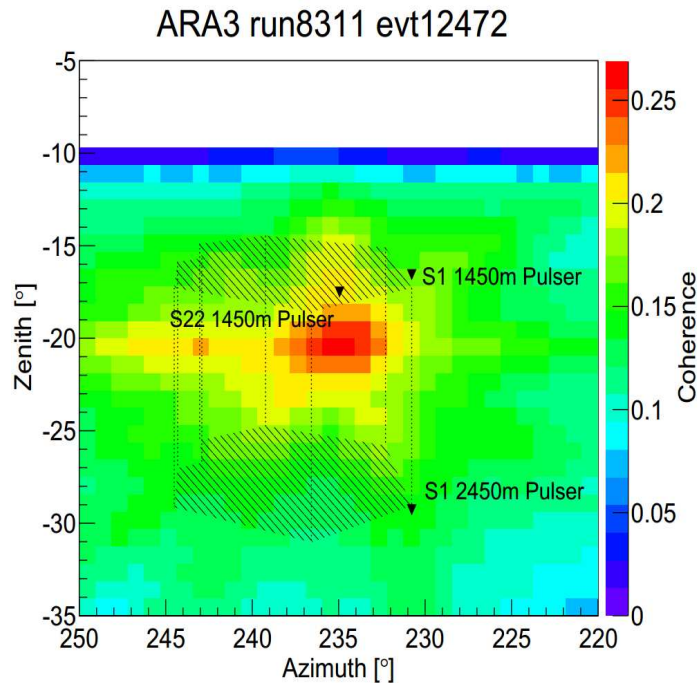


Figure 5: Reconstruction of the “sky” position of ICS22 as seen from ARA-3. The methods are described in the ARA analysis presentation to this conference[.]. This reconstruction uses just the Vpol QD rays, but otherwise assumes the station and array geometry and icemodel described herein. The raytracing for reconstruction is table driven, as described in [9].

an “image” station above the ice surface, the baseline for reconstruction by both rays is of order twice the depth of the station, or 400m. A full 3D reconstruction is then possible. To illustrate this, we extract two pulse snips from each waveform, perform the correlations between snips, and identify the time lag between pairs of pulses from the location of the peak in the envelope function. These δt_{ij} are compared to predicted separations for a hypothetical source location. The rms of the residuals across all pairs is computed as a score for the considered location. Figure 6 shows the result of this procedure from varying the distance, zenith, and azimuth in three independent 1D scans. Distance to the vertex is resolved to about 100 m. The zenith angle is determined with a baseline of 400 m, and is quite tight, whereas the azimuthal baseline is still 20 m and fairly loose.

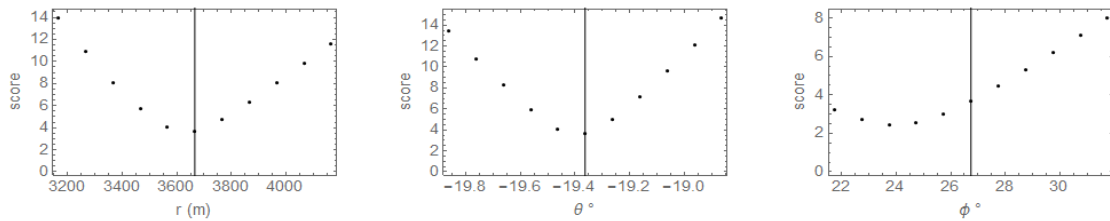


Figure 6: 1D scans in distance, zenith and azimuth for RMS timing residuals as the deep pulser position is adjusted. The true position lies near the minimum of the scans. These scans include information from both rays, which greatly improves the distance resolution (see text).

3. Evidence for birefringence

As mentioned earlier, Figure 3 shows Hpol signals that arrive before the corresponding Vpol signals. For example, consider S1TV and S1TH, top Vpol and top Hpol on string 1. The Vpol antenna is about 3m below the Hpol antenna, and yet the upcoming QD signal arrives at the Hpol antenna about 30 ns ahead of the Vpol signal. Similarly, the QR pulse is also seen on Hpol antennas and also leads. In addition, the Hpol channels show a secondary pulse which appears at about the same time as the corresponding Vpol. To explore this, snips were acquired for the Hpol pulses, and cross-correlation and envelope functions were produced to determine the relative timing. The left/right panels of Figure 7 show the results for QD/QR. The peaks of the envelope function are displaced by about 30 ns from the expected arrival time separation. In addition to the displaced main peak of the envelope, both correlations show a secondary peak near the expected arrival time, a feature consistent with the direct observation of the waveforms. The situation is somewhat obscured, however, by features of the main Vpol pulse. The deep pulser waveforms have a width of about 42 ns, with pronounced leading and trailing edges which create features in the correlation functions (e.g. see the green QR:QD section in Figure 4). These features overlay possible features from a second pulse. The result is an H-V envelope function that has two wings at $\pm 30 - 40$ ns, but with asymmetric amplitudes.

There are 13 channels where an H-V correlation can be determined, 8 are QD and 5 are QR. The three missing QR cases correspond to cases where the waveform for the Vpol antenna ends before the arrival of the QR pulse. This happens on the channels which are further away from the deep pulser (string 3, and the bottom antenna on string 1). After resolving peak confusion, the Hpol advance for all 13 cases is in the range of 30-35 ns, as shown in Figure 8.

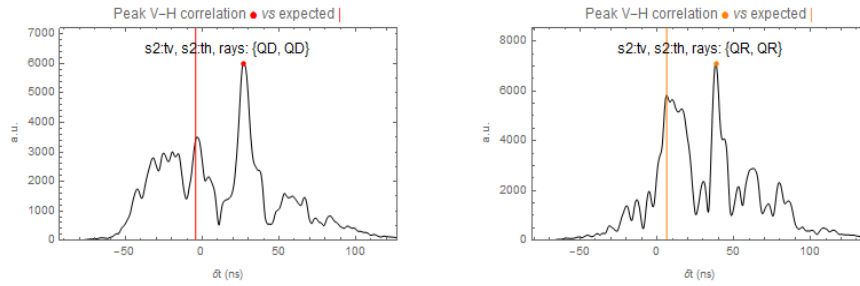


Figure 7: Left: Cross-correlation of waveform snips for QD pulses observed in top Vpol and Hpol antennas, showing the lag corresponding to the peak in the correlation and the *expected* lag time if both Vpol and Hpol shared a common index of refraction. Right: Same, but for QR pulses. In both cases the Hpol signal arrives about 32 ns ahead of expectations. Note that the physical arrival time lags are different by -4 and +6 ns for the two cases, since the QD is upcoming and the QR is down going. Also visible are secondary peaks due to the intrinsic shape of the deep pulser waveforms and, apparently, a secondary peak in Hpol coincident with the arrival of the Vpol signal (see text).

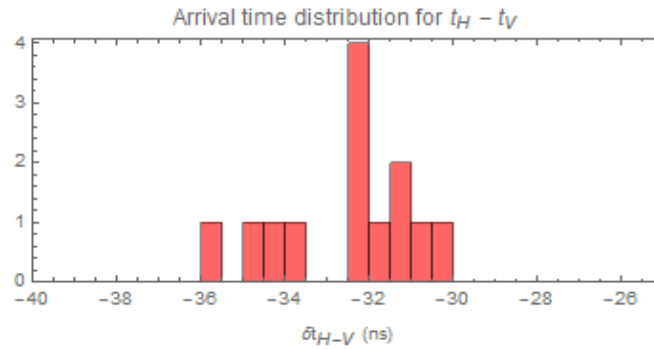


Figure 8: Histogram of time lags for equivalent QD or QR pulses in both Hpol and Vpol. Three antennas have had the identified peak of the correlation function adjusted to resolve source confusion.

The source of the Hpol is uncertain. Possibilities include antenna cross-pol emission and response, eigenstates that are rotated or mixed with respect to nominal V & H, and mixing in flight. A common advance for all 13 cases argues against cross-talk in the DAQ. The similar amplitude of initial and secondary Hpol pulses could result from cross-pol emission, followed by birefringent propagation. At the station, the slower Vpol ray would be picked up by similar cross-pol response by the receiving antennas. Rotation of the polarization vectors for the propagating eigenstates would produce similar effects for cross-pol in any H-V antenna system.

4. Discussion and plans for use of SPICE Core

ARA observations of the deep pulsers confirm the paradigm of geometric optics for RF propagation through ice. This result is especially interesting in the context of reports of horizontal propagation of RF signals, even in the presence of a gradient to the index of refraction. Such propagation could occur if there are density layers in the firm. A density inversion could produce a horizontal waveguide where radiation is confined by refraction, similar to an optical fiber with a

graded index of refraction. Similarly, weak discontinuities in density can result in scattering surfaces for highly inclined rays, producing a channel for horizontal propagation. Our results show that, at least for depths below 65 m, these effects do not dominate over geometric optics. At the same time, close examination of Figure 3 shows that while the QD rays have sharp leading edges, the QR rays have precursors consistent with a picture where the path for the upper part of the QR ray can be shortened via a horizontal propagation of part of the signal power.

The evidence for birefringence must be interpreted in the context of previous results. Ref. [10] observes birefringence in vertical propagation of rays which reflect off the bedrock. They conclude that the time delays accumulate mostly in the deep ice, below about 1200 m, but observe no evidence for birefringence in the upper ice. This is consistent with a crystal orientation fabric (COF) determined by shear in the ice flow, which is rather modest in the upper ice. The current results, however, suggest that the upper ice does exhibit birefringence. If the COF of the upper ice is dominated by gravity, then a vertical ray would not exhibit birefringence, but a horizontal ray would since the Vpol would be along the net c-axis while Hpol would be transverse to it.

The observations presented here are a small part of the radio-glaciological data needed to fully characterize RF propagation of relevance to the ARA experiment. In this regard, within the last two years, a 1700-m deep ice core was extracted from the South Pole ice. The data provided by that core, and its importance for neutrino detection, is currently under study by ARA. More importantly, the hole itself is located at distances of 0.5-several km from current and planned ARA stations, providing a unique opportunity to survey the ice as a function of depth and test RF propagation models against known ice characteristics. To this end, the ARA collaboration has been granted access to the SPICE hole for the 2017-18 and 2018-19 austral seasons, and are planning an extensive set of tests using transmitters lowered into that icehole. Key observations include confirmation of a classical shadow zone due to the varying index of refraction, demonstration of horizontal propagation in the firm, and birefringence as a function of depth and incident angle. In addition to the deep ARA stations, data will also be collected by a surface station duplicating the ARIANNA[11] design, but deployed at South Pole, providing data specific to horizontal propagation in the shallow firm.

References

- [1] P. Allison et al. (ARA Collaboration), *Phys. Rev. D* 93, 082003 (2016).
- [2] P. Allison et al. (ARA Collaboration), *Astropart. Phys.* 70, 62 (2015).
- [3] P. Allison et al. (ARA Collaboration), *Astropart. Phys.* 88, 7-16 (2017).
- [4] M.-Y. Lu et al. (ARA collaboration), *Proceedings 35th ICRC (2017)*, PoS(ICRC2017)966.
- [5] P. Allison et al, (ARA collaboration), *Proceedings 35th ICRC (2017)*.
- [6] P. Allison et al. (ARA), *Astropart. Phys.* 35, 457 (2012).
- [7] S. Barwick, D. Besson, P. Gorham, and D. Saltzberg, *Journal of Glaciology* 51, 231 (2005).
- [8] T. Meures, PhD Dissertation, Univ. Libre de Bruxelles (2014).
- [9] M. Beheler-Amass et al. (ARA collaboration), *Proceedings 35th ICRC (2017)*, PoS(ICRC2017)1054.
- [10] D. Besson, I. Kravchenko, A. Ramos, J. Remmers, *Astropart. Phys.* 34, 10 (2011).
- [11] S. Kleinfelder, Presented at 2015 IEEE Nuclear Science Symposium (2015), [arXiv:1511.07525].